β1 integrin regulates alveolar epithelial cell differentiation following injury

Jennifer M.S. Sucre[1,4], Fabian Bock[2], Nicholas M. Negretti[1], John T. Benjamin[1], Peter M. Gulleman[1], Xinyu Dong[2], Kimberly T. Ferguson[1], Christopher S. Jetter[1], Wei Han[3], Yang Liu[3], Seunghyi Kook[1], Jason Gokey[3], Susan H. Guttentag[1], Jonathan A. Kropski[3,4,5], Timothy S. Blackwell[3,4,5], Roy Zent[2,4,5], Erin J. Plosa[1*]

[1] Department of Pediatrics, Division of Neonatology, Vanderbilt University Medical Center, Nashville, TN 37232, USA
[2] Department of Medicine, Division of Nephrology and Hypertension, Vanderbilt University Medical Center, Nashville, TN 37232, USA
[3] Department of Medicine, Division of Allergy, Pulmonary, and Critical Care Medicine, Vanderbilt University Medical Center, Nashville, TN 37232, USA
[4] Department of Cell and Developmental Biology, Vanderbilt University Medical Center, Nashville, TN 37232, USA
[5] Nashville Veterans Affairs Medical Center, Nashville, TN 37232, USA

Address Correspondence to
Erin Plosa
2215B Garland Avenue
1125 MRB4/ Light Hall
Vanderbilt University Medical Center
Nashville, TN, 37232
(erin.plosa@vumc.org)
615-343-4876

The authors have declared that no conflict of interest exists.

Abstract

β1 integrins are known to regulate lung development and homeostasis, however their role in lung epithelial repair is unclear. In this study, we challenged mice with a type 2 alveolar epithelial cell deletion of β1 integrin with a single dose of intratracheal lipopolysaccharide. These mice developed persistent inflammation, severe lung injury, and emphysema. The β1 integrin-deficient alveolus repaired by repopulating with overabundant large, round type 2 alveolar epithelial cells and reduced numbers of alveolar type 1 cells. These abnormal β1 integrin deficient type 2 cells had significant actin cytoskeletal defects resulting in their inability to attain a flattened type 1 cell shape. In addition, terminal differentiation into type 1 and 2 alveolar epithelial cells was impaired as they expressed both type 2 and intermediate cell markers. Thus, β1 integrin plays a key role in alveolar repair by regulating the cell-shape change required for type 2 to type 1 epithelial differentiation.

Introduction

Integrins are heterodimeric transmembrane protein receptors comprising an α and β subunit that bind extracellular matrix (ECM) ligands. Integrins provide a physical connection between cells and the ECM, propagating signaling to and from the surrounding matrix (1-3). Of the 24 integrin heterodimers, 12 contain the β1 subunit, and many are present in epithelial tissues. Integrins regulate critical epithelial cell processes such as adhesion, migration, proliferation, differentiation, and cell survival during morphogenesis of branched organs (4, 5). β1 integrins which include the collagen IV and laminin receptors, are required for lung development and they regulate alveolar homeostasis post-development; however, the role of β1 integrin in regulating injury-repair is unknown.

The alveolar basement membrane, which is primarily comprised of collagen IV and laminin, facilitates gas exchange between airspace and capillaries. The alveolar basement membrane is covered by cuboidal type 2 alveolar epithelial cells (AT2 cells) and thin, elongated type 1 alveolar epithelial cells (AT1 cells), each with essential functions. AT2 cells secrete surfactant, lowering alveolar surface tension, and function in an immunoregulatory role, while the thin elongated shape of AT1 cells promotes efficient gas exchange and water homeostasis, as well as produce components of the basement membrane (6). Following injury to the distal lung parenchyma, multiple epithelial progenitors replenish the epithelium in both human lung disease and murine models (7, 8). The most mature epithelial progenitor for distal lung repair is the AT2 cell itself, which can become a transitional cell characterized by expression of genes such as *Krt8* or *Areg* (7, 9, 10) during differentiation to replace AT1 cells. Several pathways, including epidermal growth factor receptor pathway (EGFR), insulin-like growth factor receptor (IGFR),

fibroblast growth factor pathway, hepatocyte growth factor (HGF) pathway, wingless/integrated (Wnt) pathway, and yes-associated pathway 1 (YAP) signaling (11-15), drive AT2 progenitor cell proliferation. The proliferation of AT2 cells is restrained by various proteins including the tight junction protein Claudin-18 (15). The final point of transition in alveolar repair is the acquisition of AT1 transcriptional phenotype and a flat elongated cell shape that facilitates gas exchange by diffusion.

Differentiation from AT2s into AT1s requires a substantive change in cell shape. For a cuboidal AT2 cell to thin and elongate to cover an injured basement membrane, adherens junctions and focal adhesions must remodel and actin-rich cellular protrusions expand along the basement membrane in the direction of cellular extension (16). Integrin-mediated adhesion and migration utilize similar cellular processes, and we have previously reported that epithelial adhesion and migration requires β1 integrin in the developing lung. Thus, it is possible that β1 integrin-dependent epithelial cell functions play a critical role in alveolar repair.

In this study, we deleted β1 integrin in SP-C expressing AT2 cells in the adult lung post-development and induced lung injury by intratracheal instillation of *E. coli* lipopolysaccharide (LPS). β1 integrin-deficient mice exhibited increased inflammation and lung injury, followed by development of emphysema. The β1-deficient cells were unable to fully repair the epithelium after injury, with excessive proliferation of AT2 cells and failure of AT1 differentiation. Together, these studies identify an unexpected role for β1-containing integrins in regulating lung AT2 cell differentiation required for lung repair following injury.

Results

LPS-induced injury after β1 integrin deletion in AT2s results in increased inflammation, abnormal repair, and decreased survival.

To determine the role of epithelial β1 integrin in alveolar repair after injury, we challenged $\beta1^{rtTA}$ and littermate $\beta1^{f/f}$ control mice with a single intratracheal (IT) dose (3 μg/g mouse weight) of lipopolysaccharide (LPS) at 3 months of age, a time point of similar alveolar size between $\beta1^{rtTA}$ and littermate controls (**Figure 1A**) (17). $\beta1^{rtTA}$ mice exhibited decreased survival compared to $\beta1^{f/f}$ control mice (44% survival at 21 days for $\beta1^{rtTA}$ versus 93% for $\beta1^{f/f}$, **Supp. Figure 1A**), with 100% survival for both PBS treated $\beta1^{rtTA}$ and $\beta1^{f/f}$ mice (data not shown). At 3 days post-injury, histological examination revealed an expected increase in inflammatory cells in LPS-treated $\beta1^{rtTA}$ and control $\beta1^{f/f}$ lungs and markedly increased edema in $\beta1^{rtTA}$ lungs (**Figure 1A**). LPS-treated $\beta1^{f/f}$ lungs returned to a normal histological appearance by day 7, while edema and inflammation remained prominent in the $\beta1^{rtTA}$ lungs. At 21 days, $\beta1^{rtTA}$ lungs exhibited a marked increase in airspace size, along with evidence of septal destruction. Emphysema was quantified by increased mean linear intercept (28.5±0.9 μm in $\beta1^{f/f}$ lungs vs. 40.2±2.8 μm in $\beta1^{rtTA}$ lungs) (**Figure 1B**). To evaluate alveolar barrier function, we measured bronchoalveolar lavage (BAL) fluid protein levels at all timepoints (**Figure 1C**). $\beta1^{rtTA}$ BAL fluid contained increased protein in the unchallenged state, as well as at 3 and 7 days post-LPS compared to control $\beta1^{f/f}$ BAL fluid. By 21 days post-injury, protein levels were similar in both mouse strains, indicating restoration of alveolar barrier function in $\beta1^{rtTA}$ lungs.

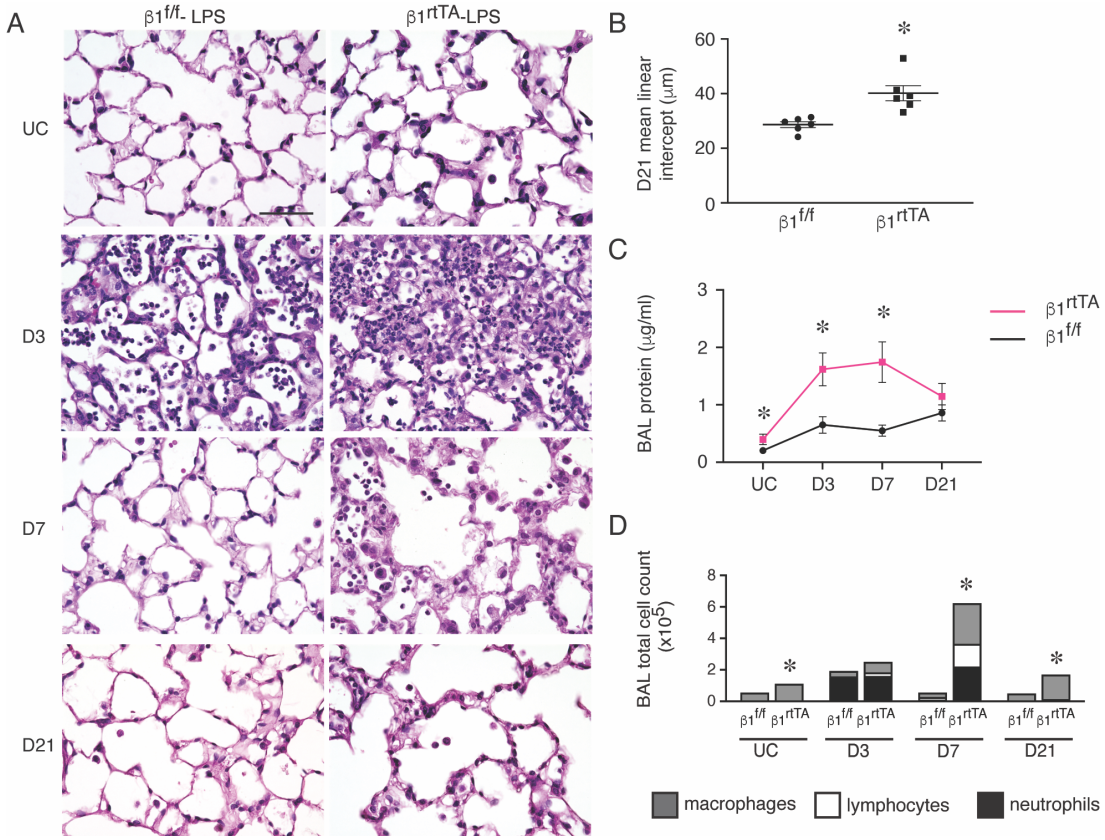

Figure 1. β1 integrin deletion in AT2s results in increased inflammation, abnormal repair, and decreased survival after LPS-induced injury. (A) Representative images of lung histology demonstrate increased edema at 3 and 7 days post-injury in $\beta1^{rtTA}$ lungs compared to $\beta1^{f/f}$ lungs, as well as persistent inflammation and emphysematous remodeling in $\beta1^{rtTA}$ lungs by 21 days post-LPS. (B) Mean linear intercept quantified emphysematous alveolar remodeling at 21 days post-LPS, 28.5±0.9 μm in $\beta1^{f/f}$ lungs vs. 40.2±2.8 μm in $\beta1^{rtTA}$ lungs (n=6-7 mice/ group, p=0.0014 by two-tailed t-test). (C) Bicinchoninic Acid protein assay quantified increased bronchoalveolar lavage (BAL) fluid protein in unchallenged (UC) $\beta1^{rtTA}$ lungs and at 3 and 7 days post-LPS injury in $\beta1^{rtTA}$ lungs compared to $\beta1^{f/f}$ lungs at the same timepoints (n=6-14 mice/ group, two-tailed t-test comparing genotypes at each time point, p=0.0485 for UC mice; p=0.0036 at D3; p=0.005 at D7; p=0.2628 at D21). (D) BAL cell counts are significantly increased in $\beta1^{rtTA}$ lungs compared to $\beta1^{f/f}$ littermates in UC mice and at 7 and 21 days post-LPS. Peak inflammation is present at 7 days in $\beta1^{rtTA}$ lungs, 55,663±3306 cells/ ml in $\beta1^{f/f}$ BALF versus 624,000±118,753 cells/ml in $\beta1^{rtTA}$ BAL (n=6-26 mice/group, two-tailed t-test comparing genotypes at each time point, p=0.0002 for UC mice; p=0.0730 at D3; p=0.0007 at D7; p<0.0001 at D21). Total numbers of BALF macrophages are significantly increased in UC $\beta1^{rtTA}$ mice and at day 7 and day 21, lymphocytes and neutrophils are significantly increased in $\beta1^{rtTA}$ BAL at day 7 only. Scale bar=50 μm for (A). $* \; p < 0.05$

We collected BAL fluid to characterize the inflammatory response to LPS and found no significant differences in immune/ inflammatory cells between $\beta1^{rtTA}$ and $\beta1^{f/f}$ lungs at 3 days, during the expected peak of inflammation following LPS (18) (**Figure 1D**). However, in $\beta1^{rtTA}$ mice, there was a delayed inflammatory peak at 7 days post-injury characterized by persistently

increased neutrophils in BAL fluid from $\beta1^{rtTA}$ lungs (**Supp. Figure 1B**). Although the BAL cell count decreased towards baseline at 21 days in $\beta1^{rtTA}$ lungs, increased numbers of macrophages were identified at this timepoint. This finding was confirmed by quantification of immunostaining for the macrophage marker CD68 (**Supp. Figure 1C-E**). These findings indicate that persistent inflammation in lungs of β1-deficient mice may contribute to development of emphysema in this model.

Expansion of β1 deficient AT2 population in $\beta1^{rtTA}$ lungs after injury.

To determine whether β1 deficient epithelial cells contribute to abnormal repair, we performed an in-depth histological and transcriptomic examination of alveolar epithelial cells in $\beta1^{rtTA}$ and $\beta1^{f/f}$ lungs. Lung sections immunostained for the AT2 marker pro-SP-C and AT1 marker T1α demonstrate accumulation of pro-SP-C+ AT2s in $\beta1^{rtTA}$ lungs by day 7 following LPS injury (**Figure 2A**). By day 21, the alveolar septa were lined by abundant pro-SP-C+ AT2s, accompanied by decreased expression of T1α in $\beta1^{rtTA}$ lungs, suggesting loss of AT1s and expansion of the AT2 population over time during alveolar repair. Despite the inherent difficulties in AT1 quantification by histology, we captured the expanding imbalance between AT2 cells and AT1 cells in $\beta1^{rtTA}$ lungs by calculating the number of pro-SP-C+ cells as a percent of total cells. Whereas the percent of AT2 cells remained stable from day 3 into late repair in the $\beta1^{f/f}$ lungs, the percent of pro-SP-C positive AT2 cells increased progressively throughout the later timepoints of repair in $\beta1^{rtTA}$ lungs (**Figure 2B**). The increased number of AT2 cells in $\beta1^{rtTA}$ lungs prompted an examination of proliferation and apoptosis. We assessed changes in AT2 proliferation by co-immunostaining lung sections for the proliferation marker Ki67 with pro-SP-C. $\beta1^{rtTA}$ lungs exhibited increased proliferation in pro-SP-C+ AT2 cells at all

sampled timepoints from unchallenged lungs to day 21 after injury, with peak proliferation at day 7 (**Figure 2C-D**). We next analyzed cell survival by TUNEL assay co-immunostained with pro-SP-C. Although we identified a small but significant increase in the total number of apoptotic cells per field in $\beta1^{rtTA}$ lungs on day 7 and 21 after LPS (**Figure 2E-F**), apoptosis was significantly increased in β1 deficient AT2s only on day 21 (**Figure 2G**), suggesting that epithelial apoptosis was not the major causative factor in emphysema development.

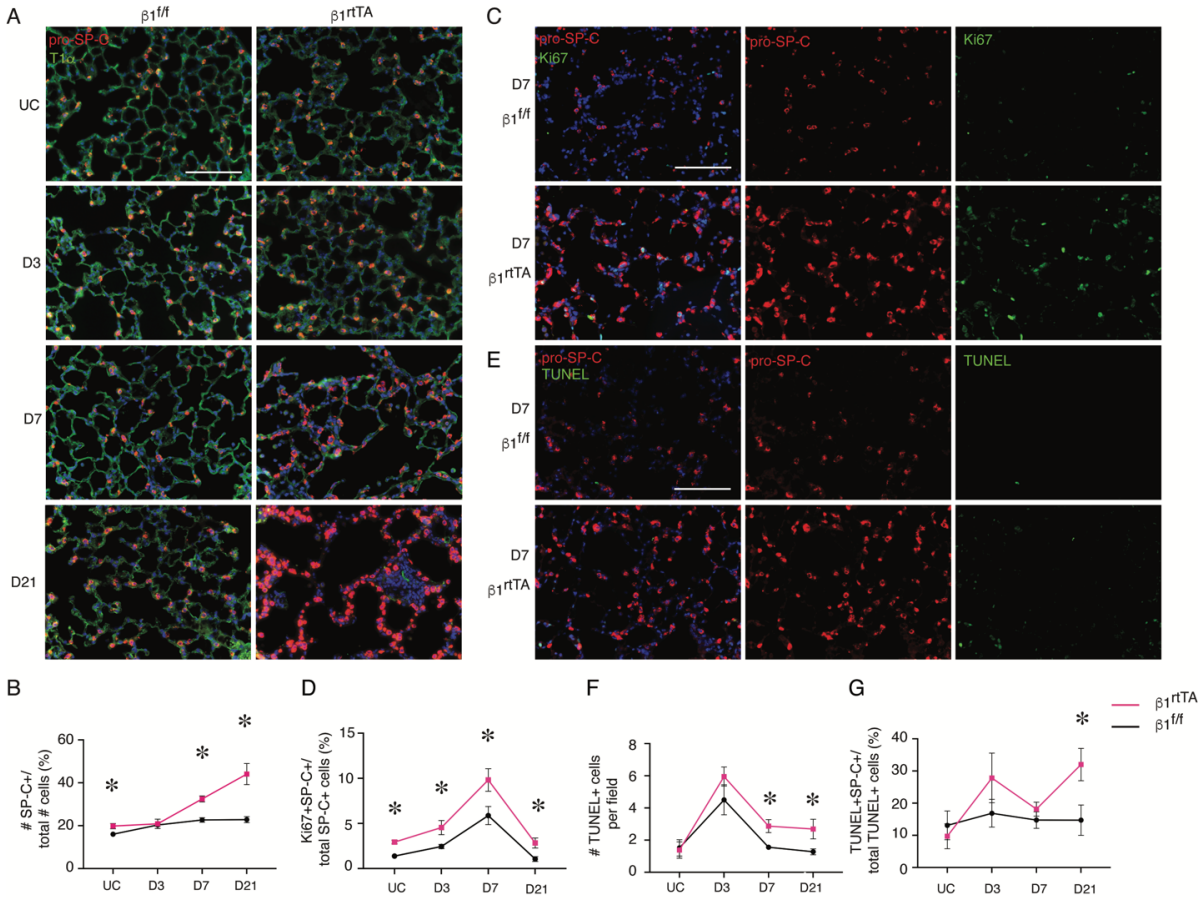

Figure 2. β1 deficient AT2 population expands in $\beta1^{rtTA}$ lungs after injury. (A) Lung sections immunostained for pro-SP-C (red) and T1α (green) demonstrate increased AT2 cells and decreased T1α expression in $\beta1^{rtTA}$ lungs by day 7 after LPS injury. (B) Quantification by percent of number pro-SP-C+ cells per total cells (n=6-8 mice/ group, *p*=0.0247 for UC mice; *p*=0.8220 at D3; *p*=0.0001 at D7; *p*=0.0009 at D21, 5 sections per mouse). (C) Lung sections immunostained for the proliferation marker Ki67 (green) and pro-SP-C (red) show peak proliferation of AT2s in $\beta1^{rtTA}$ lungs at day 7, with single color panels for pro-SP-C and Ki67 as indicated. (D) Quantification of proliferating AT2 cells by percent of total pro-SP-C+ AT2s (n=6-8 mice/ group, *p*=0.0003 for UC mice; *p*=0.0311 at D3; *p*=0.0310 at D7; *p*=0.0128 at D21, 10 sections/ mouse). (E) TUNEL/ pro-SP-C immunostaining demonstrates low levels of apoptotic AT2s at day 7 in $\beta1^{rtTA}$ lungs. (F) Quantification of total TUNEL+ cells per field shows small but significant increase in apoptotic cells on days 7 and 21 (n=6-18 mice/ group, *p*=0.8596 for UC mice; *p*=0.2184 at

D3; p=0.0011 at D7; p=0.0439 at D21, 10 sections/ mouse). (G) Quantification of TUNEL/pro-SP-C dual + cells per total number TUNEL+ cells shows a modest increase in apoptotic AT2 cells at day 21 (n=6-18 mice/ group, p=0.5867 for UC mice; p=0.2436 at D3; p=0.3688 at D7; p=0.0246 at D21, 10 sections/ mouse) $* p < 0.05$. Scale bar = 100 μm for A, C, and E. Two-tailed t-test used to compare genotypes at each time point for B, D, F, and G.

Overabundant AT2s are transcriptionally distinct during repair in β1^{rtTA} mice.

To investigate the transcriptional phenotype of β1 deficient epithelial cells that could explain the development of emphysema and other features of abnormal repair in β1^{rtTA} mice, we performed single-cell RNA sequencing (scRNAseq) on unchallenged and LPS-treated β1$^{f/f}$ and β1^{rtTA} lungs, 7 days after LPS exposure. From single-cell lung suspensions from digested whole lung (n= 3-4 mice/ group pooled into a single sample for each condition), we collected CD45-/Ter119- viable cells by fluorescence-activated cell sorting (FACS), thereby excluding immune cells and red blood cells. Single-cell RNA-sequencing was performed using the 10x Genomics platform. After doublet removal, normalization, and scaling, we isolated 2,926 epithelial cells for analysis. Initially, we analyzed our transcripts with a label transfer technique utilizing the epithelial markers reported by Strunz et al during bleomycin-induced injury-repair in mice (7). In both injured and unchallenged mice, we found all major alveolar epithelial populations in both β1^{rtTA} and β1$^{f/f}$ lungs, indicating the validity of this methodology (**Figure 3A**). AT1 cells were isolated in low abundance, likely due to cell loss because of their relatively fragile structure (19). UMAP embedding identified a distinct epithelial population in β1^{rtTA} lungs at 7 days after injury (**Figure 3B**). Visualizing the UMAPs of the four individual groups, most of the epithelial cells were classified as AT2s or activated AT2s in LPS-treated β1^{rtTA} lungs and mapped to transcriptionally distinctly clusters; however, we combined these groups (AT2/activated AT2 cells) for further analysis. To identify potential β1 integrin-dependent pathways that regulate AT2 to AT1 differentiation during repair, we examined the top differentially expressed genes by Ingenuity Pathway Analysis in the combined AT2 cell group between unchallenged and LPS-

treated β1^{rtTA} and β1$^{f/f}$ mice (**Figure 3C-D** and **Supp. Figure 2A-B**). In unchallenged mice, the most enriched pathways with injury were an upregulation of the oxidative stress response pathway in β1^{rtTA} AT2 and activated AT2 cells, followed by senescence, JAK/STAT, and IL-6 signaling pathway upregulation. All 4 of these pathways are relevant to development of emphysema (20, 21). In the injured lungs, the top 8 differentially up-regulated pathways included regulatory signaling networks related to adherens junctions, the actin cytoskeleton, and Rho GTPases. Since remodeling of adherens junctions is a necessary step in elongation of cell shape and Rho GTPases are known intermediary signaling effectors between integrins and the actin cytoskeleton, these data suggest that β1 integrin regulates the transition in cell shape during AT1 cell differentiation.

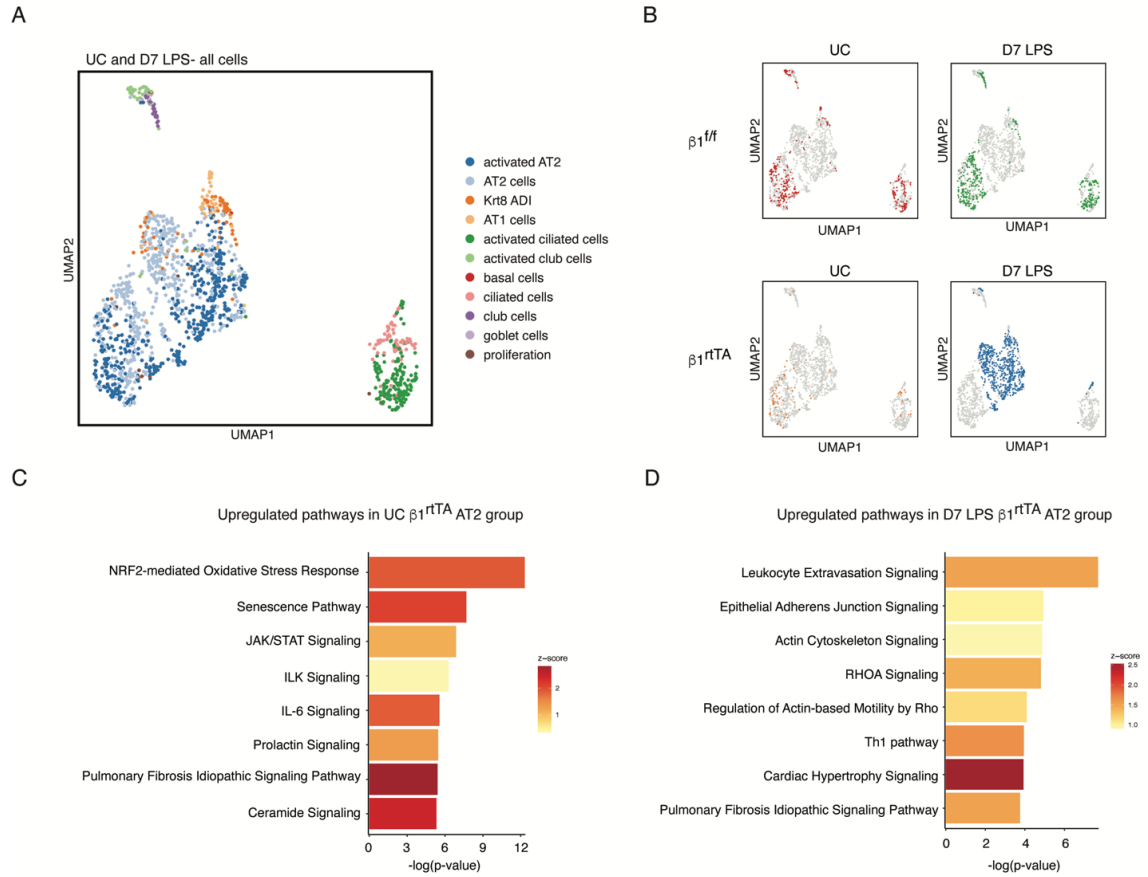

Figure 3. Overabundant AT2s are transcriptionally distinct during repair in β1^{rtTA} mice. (A) UMAP of all epithelial cells from β1$^{f/f}$ and β1^{rtTA} lungs ± LPS clustered by label transfer from Strunz et al (7). (B) Individual epithelial populations by group reveal transcriptionally distinct AT2s and activated AT2s in day 7 LPS-treated β1^{rtTA}

lungs. (C) Ingenuity Pathway Analysis on combined AT2 groups from unchallenged $\beta1^{f/f}$ and $\beta1^{rtTA}$ lungs demonstrate upregulation of oxidative stress, senescence, and inflammatory pathways in $\beta1^{rtTA}$ lungs. (D) Ingenuity Pathway Analysis shows upregulation of actin cytoskeleton signaling pathways at 7 days after LPS treatment.

β1 integrin regulates actin expression and RhoA GTPase activation during alveolar repair.

To investigate how β1 integrin regulates the actin cytoskeleton during alveolar repair, we imaged thick frozen sections immunostained for F-actin phalloidin with pro-SP-C. Our histological analysis showed that injured $\beta1^{f/f}$ pro-SP-C+ AT2 cells formed actin-based protrusions at the areas of lateral extension the cells (arrows in **Figure 4A**), as described in differentiating epithelial progenitors during development (22). In contrast, AT2s in injured $\beta1^{rtTA}$ lungs exhibited a large, rounded cell shape with F-actin localized to the cell membrane. When we quantified the AT2 cell size by calculating the cell area, there was a significantly increased area in injured $\beta1^{rtTA}$ lungs (66.8±3.0 μm^2) compared to $\beta1^{f/f}$ lungs (48.4±1.8 μm^2) (**Figure 4B**). Since our scRNA-seq data suggested upregulation of actin cytoskeleton signaling pathways, we next applied a G-actin probe, JLA20, along with F-actin phalloidin and pro-SP-C to identify differences in actin remodeling (**Figure 4C**). We found increased amounts of both G-actin and F-actin in injured $\beta1^{rtTA}$ lungs, with F-actin primarily localized to the cell membrane (arrowheads in Figure 4C) in the $\beta1^{rtTA}$ lungs. We confirmed the increased amount of G- and F-actin by calculating the relative fluorescence of the JLA20 and phalloidin probes in pro-SP-C+ cells using corrected total cell fluorescence, which normalizes fluorescence to total cell area (**Figure 4D**). Actin remodeling and localization is mediated in part by the cytoskeletal protein ezrin. We therefore examined the localization of ezrin in injured Cre+ $\beta1^{WT/WT}$ littermates and $\beta1^{rtTA}$ mice crossed to the mTmG Cre recombinase reporter (with cells derived from Cre recombinase active AT2s labeled in green). Ezrin expression (white) localized to the points of lateral extension in control mice (arrows in **Figure 4E,** high power white single channel on right panel), while ezrin

was found diffusely in AT2s in $\beta1^{rtTA}$ lungs, suggesting impaired ability to direct actin localization. Since actin remodeling is mediated by small GTPases (23), and our scRNA-seq pathway analysis reported upregulation of actin cytoskeleton signaling in AT2s from injured $\beta1^{rtTA}$ mice, we validated this finding at the protein level utilizing the GTPase assay. As predicted by our transcriptomic data, AT2 cells from injured $\beta1^{rtTA}$ lungs exhibited increased RhoA and Cdc42 GTPase activation (**Figure 4F-G**). In contrast, GTPase activation was decreased for Rac1 (**Figure 4H**), a related GTPase that play a role in formation of smaller actin-based structures. Taken together, these data indicate β1 integrin is a critical modulator for RhoA and Cdc42 GTPase activation in AT2 cells and is required for proper actin expression and localization in differentiating AT2 cells during repair.

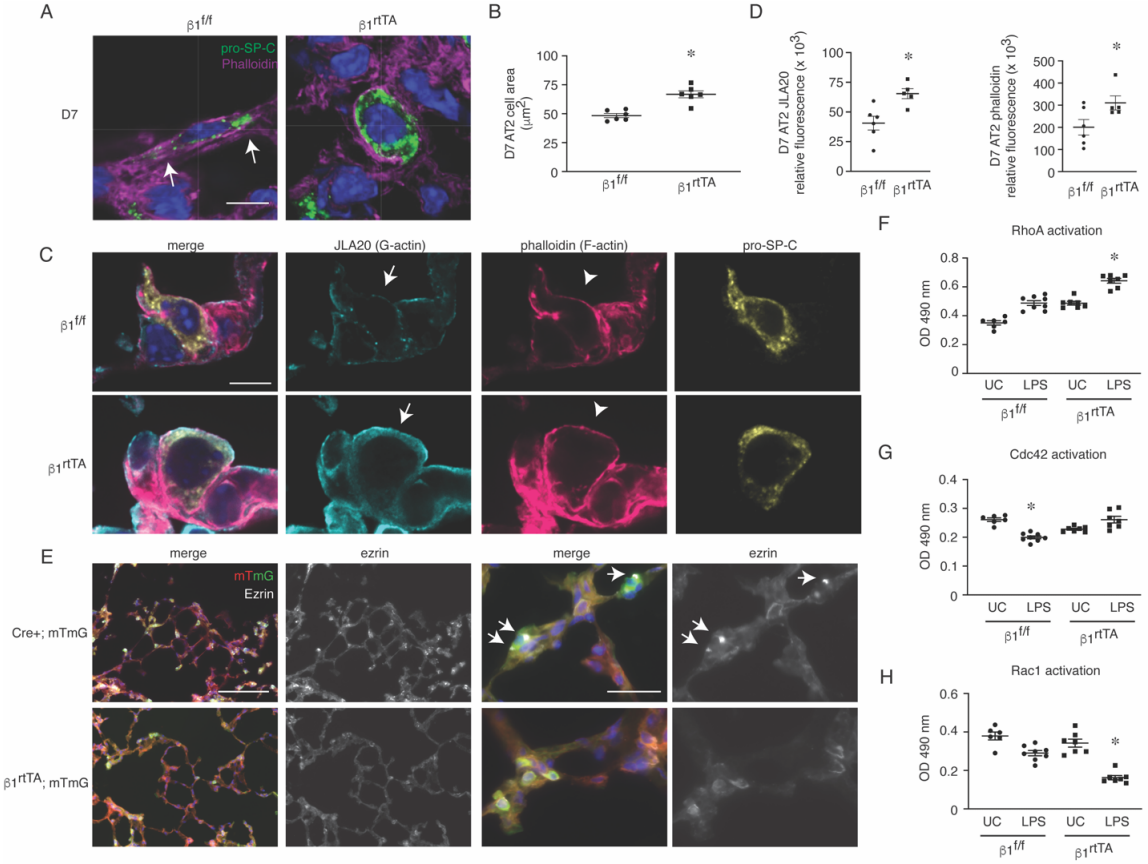

Figure 4. β1 integrin is required for change in AT2 cell shape and GTPase activation during alveolar repair. (A) High-power images of thick frozen sections from day 7 LPS-treated $\beta1^{f/f}$ and $\beta1^{rtTA}$ lungs immunostained for pro-SP-C (green) with phalloidin F-actin probe (magenta), arrows indicate areas of actin-rich lateral protrusions. (B)

Area of pro-SP-C+ AT2 cells from day 7 LPS-treated $\beta1^{f/f}$ and $\beta1^{rtTA}$ mice (48.4±1.8 μm^2 in $\beta1^{f/f}$ lungs compared to 66.8±3.0 μm^2 in $\beta1^{rtTA}$ lungs, ≥ 40 cells measured/ mouse imaged from 3 different sections, n = 6 mice/group, two-tailed t-test with p=0.0004). (C) High-power images of frozen sections prepared from day 7 injured $\beta1^{f/f}$ and $\beta1^{rtTA}$ lungs immunostained for pro-SP-C with JLA20 and phalloidin probes applied to detect G-actin and F-actin, respectively. Membrane localization of G-actin denoted by arrows and F-actin by arrowheads. (D) Quantification of JLA20 and phalloidin expression in pro-SP-C+ AT2 cells in $\beta1^{f/f}$ and $\beta1^{rtTA}$ lungs 7 days after LPS (10 sections/ mouse, n = 5-6 mice/ group, two-tailed t-test with p=0.0088 for JLA20 and p=0.0482 for phalloidin). (E) Representative low (left 2 panels) and high-power (right 2 panels) images from day 7 LPS-treated $\beta1^{f/f}$ and $\beta1^{rtTA}$ lungs immunostained ezrin (white) from $\beta1^{f/f}$ and $\beta1^{rtTA}$ mice crossed to mTmG Cre-recombinase reporter. Arrows indicate ezrin expression localized to lateral extensions in $\beta1^{f/f}$ AT2 cells, absent in $\beta1^{rtTA}$ AT2 cells. (F-H) GTPase activation assay performed on AT2 cell lysates collected from unchallenged and day 7 LPS-treated $\beta1^{f/f}$ and $\beta1^{rtTA}$ lungs (n=6-8 mice/ group for each assay; RhoA one-way ANOVA p<0.0001, F value 53.42, df=3; Cdc42 one-way ANOVA p<0.001, F value 17.46, df=3; Rac1 one-way ANOVA p<0.0001, F value 31.09, df=3). ∗ $p < 0.05$. Scale bar = 5 μm for A and C, 100 μm for low power panels and 10 μm for high power panels in E.

β1 deficient AT2s exhibit a mixed epithelial transcriptomic phenotype during alveolar repair.

Our histological analysis showed increased AT2 cells and decreased AT1 markers by immunostain (Figure 2A), suggesting significant impairment in AT2 to AT1 differentiation during repair. To define the epithelial differentiation defect at the transcriptional level we defined the percentage of lung epithelial cell types as previously defined by Strunz et al (7). As we previously published there was an increased percentage of AT2 and activated AT2 cells in the $\beta1^{rtTA}$ mice. In addition, consistent with our histology (Figure 2A), there was a significant increase in AT2 cells in the injured $\beta1^{rtTA}$ lungs, but not $\beta1^{f/f}$, at day 7 (**Figure 5A**). We next investigated the role of β1 integrin in alveolar epithelial differentiation by comparing the AT2, AT1, and keratin 8 positive intermediate cell transcriptional profiles in our unchallenged and injured $\beta1^{rtTA}$ and $\beta1^{f/f}$ lungs. Strunz et al defined the intermediate cells as Krt8 ADI cells, a transitional cell with features of both AT1 and AT2 present during alveolar repair. Both unchallenged and injured $\beta1^{rtTA}$ and $\beta1^{f/f}$ AT2/ activated AT2 cells expressed typical AT2 markers, *Sftpc, Sftpa1,* and *Abca3*, as expected (**Figure 5B**). The Krt8 ADI markers (*Krt8, Hbegf,* and *Areg*) were also moderately increased in the unchallenged $\beta1^{rtTA}$ lungs and this was

accentuated following injury. There was minimal expression of these markers in the uninjured and injured $\beta1^{f/f}$ lungs. Finally, unchallenged $\beta1^{rtTA}$ AT2/ activated AT2 cells exhibited enhanced expression compared to unchallenged $\beta1^{f/f}$ AT2 cells, which was also accentuated by injury. We next assessed the same alveolar epithelial markers in the Krt8 ADI population from unchallenged and injured $\beta1^{rtTA}$ and $\beta1^{f/f}$ lungs (**Figure 5C**). As anticipated, the Krt8 ADI population strongly expresses one or more of the Krt8 ADI marker genes, *Krt8, Hbegf,* and *Areg*, in all four conditions. Notably, the Krt8 ADI populations from both injured $\beta1^{rtTA}$ and $\beta1^{f/f}$ lungs expressed some AT1 markers, consistent with cells in transition towards an AT1 cell phenotype. Importantly, the $\beta1^{rtTA}$ Krt8 ADI populations intensely express AT2 markers *Sftpc*, *Sftpa1,* and *Abca3*, in both the unchallenged and injured conditions. In contrast, there is only scant expression of these markers retained in Krt8 ADI cells from $\beta1^{f/f}$ lungs. The retention of AT2 markers in $\beta1^{rtTA}$ Krt8 ADI cells indicates these cells exhibit a mixed transcriptional phenotype and suggests they are programmatically delayed in the differentiation process compared to $\beta1^{f/f}$ Krt8 ADI cells. The continued expression of *Sftpc* transcriptionally in both $\beta1^{rtTA}$ AT2 and Krt8 ADI cells after injury suggest that β1 integrin is required for the signaling mechanisms that govern the loss of AT2 markers and acquisition of AT1 markers during alveolar repair. Furthermore, these data indicate that β1 integrin deficient SP-C+ epithelial cells lining the alveolar compartment during repair represent a population of cells that express a spectrum of transcriptional markers from AT2, intermediate cells, and AT1 cells.

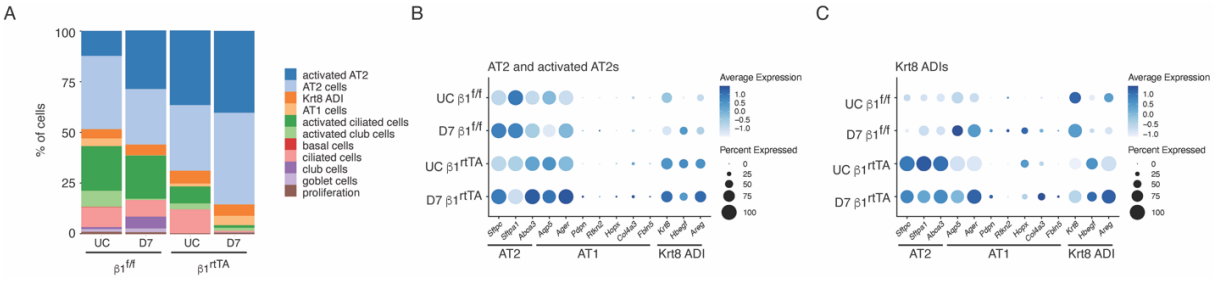

Figure 5. β1 deficient AT2s exhibit a mixed epithelial transcriptomic phenotype during alveolar repair. (A) Stacked bar graph of epithelial proportions demonstrates an expansion of the AT2 and activated AT2 populations in day 7 LPS-treated $\beta1^{rtTA}$ lungs. (B-C) Marker gene expression by genotype and treatment group in AT2/ activated AT2 and Krt8 ADI clusters, in which higher expression is represented with a darker color and the size of the dot reflects the proportion of cells expressing that marker.

AT2s of mixed transcriptomic phenotype persist, proliferate, and maintain an enlarged, rounded cell shape in late alveolar repair.

Since our histological and scRNA-seq analysis showed impaired AT2 differentiation at day 7 after LPS injury, we characterized the consequence of blocked AT2 to AT1 differentiation in late repair. As described above (Figure 3B), we performed scRNA-sequencing on unchallenged and LPS-treated $\beta1^{f/f}$ and $\beta1^{rtTA}$ lungs, 21 days after LPS exposure. To enhance detection of differentiating alveolar epithelial cell populations at this timepoint, we sequenced CD45-/Ter119- single cell lung suspensions enriched for CD326+ epithelial cells. UMAP embedding with label transfer from Strunz et al revealed transcriptional similarities between $\beta1^{f/f}$ and $\beta1^{rtTA}$ alveolar epithelial cell types (**Figure 6A-B**). By pro-SP-C/ Ki67 co-immunostaining, we demonstrated increased AT2 proliferation at day 21 during late repair (Figure 2D). Our scRNA-seq data confirmed that the AT2 population from day 21 LPS-treated $\beta1^{rtTA}$ lungs exhibited an increased G2M proliferation score compared to AT2 cells from day 21 LPS-treated $\beta1^{f/f}$ lungs (**Figure 6C**). Similar to the scRNA-seq data from day 7, we next analyzed expression of AT2, AT1, and Krt8 ADI cell markers in day 21 LPS-treated $\beta1^{rtTA}$ and $\beta1^{f/f}$ alveolar epithelial cells. We identified enhanced AT2 markers, *Sftpc*, *Sftpa1,* and *Abca3*, in AT2 and

activated AT2 cell populations from β1^{rtTA} mice compared to β1$^{f/f}$ mice (**Figure 6D**). In addition, β1^{rtTA} Krt8 ADI cells retained AT2 marker expression compared to β1$^{f/f}$ Krt8 ADI cells, exhibited markedly enhanced expression of all 3 intermediate cell markers (*Krt8, Hbegf,* and *Areg*), and increased expression of AT1 markers, *Aqp5* and *Ager*. These β1^{rtTA} Krt8 ADI cells simultaneously expressed transcriptional markers from all 3 stages of transition, providing a transcriptional rationale for the continued dysfunctional phenotype observed in β1-deficient mice. We validated the mixed transcriptional phenotype in β1^{rtTA} lungs by immunostain. In day 21 LPS-treated β1^{rtTA} lungs, markedly remodeled areas exhibited numerous pro-SP-C+/ cytokeratin 8+ cells, with occasional rounded cells that were also positive for the AT1 marker Ager (arrow in **Figure 6E**). Given the disparate cellular morphology of β1-deficient AT2 cells at earlier time points, we quantified differences in cell area in pro-SP-C+ AT2 cells. At 21 days after LPS, injured pro-SP-C+ AT2 cells from β1^{rtTA} lungs remained enlarged with a significantly increased cell area (**Figure 6F**). Since we demonstrated that cell shape is β1-dependent in AT2 cells and lateral extension is necessary for cells to transition from AT2 to AT1, we calculated a roundness score, which quantifies the degree of smooth cellular contours in an unbiased manner. Round cells possess a score closer to 1 and cells with prominent lateral extensions have a lower score towards 0 (24). The roundness score in β1$^{f/f}$ AT2 cells transiently decreased at day 3 and day 7, as they differentiated and changed shape into flattened AT1 cells. In contrast, AT2 cells from LPS treated β1^{rtTA} lungs maintained an elevated roundness score throughout repair, consistent with an inability to form lateral extensions and impaired actin remodeling (**Figure 6G**). In summary, these findings suggest that β1-dependent epithelial-matrix interactions are required for regulation of AT2 progenitor proliferation and AT2 to AT1 differentiation during

repair and loss of β1-mediated matrix interactions results in chronic persistence of epithelial cells of mixed transitional phenotype.

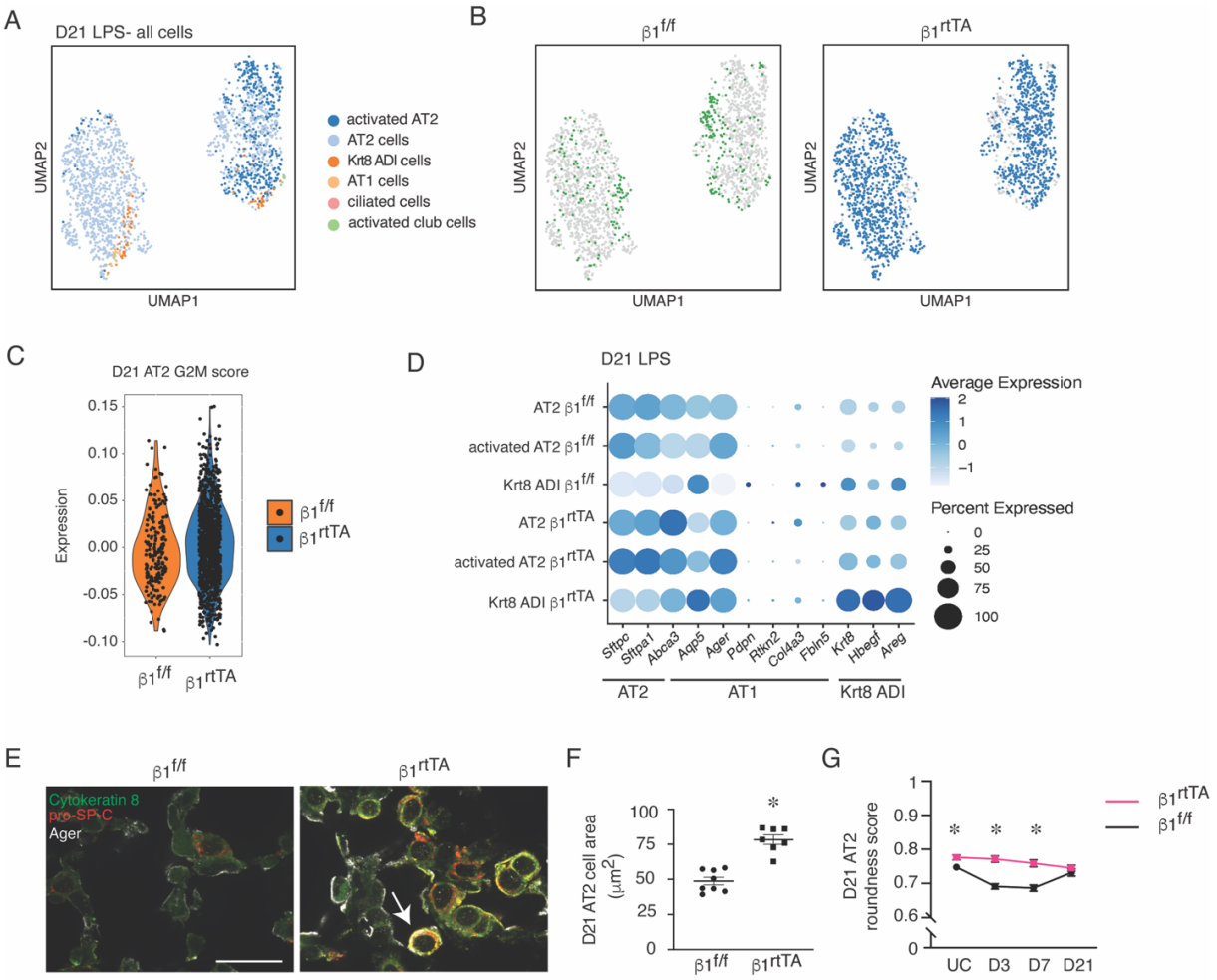

Figure 6. AT2s of mixed transcriptomic phenotype persist, proliferate, and maintain an enlarged, rounded cell shape in late alveolar repair. (A) UMAP of all epithelial cells from $\beta1^{f/f}$ and $\beta1^{rtTA}$ lungs 21 days after LPS treatment clustered by label transfer from Strunz et al (7). (B) Individual epithelial populations by group reveal transcriptionally abundant AT2s and activated AT2s in day 21 LPS-treated $\beta1^{rtTA}$ lungs. (C) G2M proliferation score demonstrates sustained AT2 proliferation at 21 days after LPS injury in $\beta1^{rtTA}$ lungs. (D) Marker gene expression by genotype in AT2, activated AT2, and Krt8 ADI clusters, in which higher expression is represented with a darker color and the size of the dot reflects the proportion of cells expressing that marker. (E) Representative high-power images of $\beta1^{f/f}$ and $\beta1^{rtTA}$ lungs 21 days after LPS co-immunostained for pro-SP-C, cytokeratin 8, and Ager. Arrow denotes occasional rounded cells co-expressing AT2, intermediate cell, and AT1 markers. (F) Area of pro-SP-C+ AT2 cells from day 21 LPS-treated $\beta1^{f/f}$ and $\beta1^{rtTA}$ mice (48.8±2.8 μm^2 in $\beta1^{f/f}$ lungs compared to 78.3±3.3 μm^2 in $\beta1^{rtTA}$ lungs, ≥ 35 cells measured/ mouse imaged from 3 different sections, n = 7-8 mice/ group, two-tailed t-test with $p<0.0001$). (G) Roundness score calculated from pro-SP-C+ cells from UC, day 3, day 7, and day 21 LPS-treated $\beta1^{f/f}$ and $\beta1^{rtTA}$ mice (≥ 35 cells measured/ mouse from at least 3 different sections, n=6-8 mice/ group, two-tailed t-test comparing genotypes at each time point, $p=0.0222$ for UC mice; $p<0.0001$ at D3; $p=0.0003$ at D7; $p=0.3641$ at D21). $* \; p < 0.05$. Scale bar = 25 μm.

Discussion

While integrins are critical for epithelial adhesion, migration, proliferation, differentiation, and cell survival during morphogenesis of branched organs (25-33), their role in epithelial repair remains unclear. In this study, we demonstrated a critical role for β1 integrin in alveolar repair after LPS-induced lung injury. β1 integrin deficient mice exhibited increased mortality due to abnormal lung repair characterized by increased inflammation and the development of emphysema. AT2 cells proliferated excessively and failed to attain AT1 cell morphology, resulting in alveoli lined by AT2-appearing cells, rather than flat AT1 cells. This was likely due to abnormalities in the actin cytoskeleton in β1 integrin deficient AT2 cells caused by dysregulated RhoA and Cdc42 GTPase signaling. These findings suggest a previously unrecognized role for β1 integrin in normal alveolar repair.

In contrast to complete recovery of wild-type mice 7 days after a single IT LPS dose, mice with β1 deficient AT2 cells demonstrated excessive death, persistent inflammation, and emphysema at 21 days after injury (34). Although airspace expansion has been reported with either 2-hit injury models or chronic repetitive low dose LPS exposure over a span of weeks or months (35-39), our β1 deficient mice are the first targeted epithelial deletion that results in subacute alveolar destruction following a single exposure to LPS, underscoring the importance of epithelial β1 integrin in alveolar repair. The development of emphysema in LPS-treated $\beta1^{rtTA}$ mice appears to be related to excessive inflammation, enhanced vulnerability of β1 deficient AT2 cells to injury, and aberrant repair mechanisms. Our scRNA-sequencing pathway analysis from unchallenged $\beta1^{rtTA}$ and $\beta1^{f/f}$ mice demonstrates the inherent susceptibility to injury with

loss of β1 integrin in AT2 cells, as it results in upregulation of oxidative stress, senescence, and inflammatory pathways, all contributing factors to emphysema pathogenesis. LPS challenged $\beta1^{rtTA}$ mice also exhibit increased inflammation during repair, an important component of COPD (40) with a sustained increase in neutrophils at day 7 after LPS, potentially making prolonged exposure to elastase a contributing factor for emphysema development. At 21 days post-injury, $\beta1^{rtTA}$ lungs retain elevated levels of macrophages, a significant source of matrix metalloproteinase-9 (MMP-9), which remodels alveolar matrix in COPD (37). LPS-treated $\beta1^{rtTA}$ lungs also exhibited increased AT2 apoptosis at day 21, which may contribute to the development of emphysema. It is unlikely that the increase in apoptosis was the primary mechanism for the development of emphysema as it was only present as day 21, when emphysematous structural changes had already occurred. In summary, the etiology for emphysematous alveolar remodeling in β1 deficient mice is likely multi-factorial with both a direct epithelial contribution and indirect effects from epithelial-driven chronic inflammation.

In this study, we provide direct evidence that β1 integrin is required for alveolar repair through regulation of actin-dependent epithelial cell shape. The role of integrins in regulating the epithelial actin cytoskeleton has been previously reported in Drosophila epithelium and murine podocytes (41-44). In these models, integrin loss limits cellular extension by misdirection of cytoskeletal components (41, 42, 45). Our scRNA-sequencing analysis supports this notion, as actin remodeling pathways were differentially expressed in injured β1-deficient AT2 cells. During development, lung epithelial cells require actin-based protrusions to attain a flattened AT1 shape (22). Our data show that loss of β1 integrin in AT2 cells enhances activation of RhoA and Cdc42 GTPases, signaling intermediaries in pathways that regulate actin polymerization.

Integrin clustering at the cell membrane determines spatial specificity of Rho GTPase signaling, an important step in actin nucleation and polymerization (46). Loss of β1 integrin could result in aberrant GTPase activation and poorly localized actin nucleation, consistent with the diffuse cytoplasmic ezrin immunostaining in LPS-treated $\beta1^{rtTA}$ AT2 cells and maintenance of a rounded cell shape.

The lung is unique among branched organs in that AT2s, which act as distal epithelial progenitors, contribute substantially to alveolar regeneration (47), whereas no distal epithelial progenitor has been reported in the kidney, mammary gland, or pancreas. Multiple signaling pathways have been implicated in the positive and negative regulation of AT2 progenitor proliferation in the adult lung, including EGF, IGF, FGF, HGF, Wnt, and Yap-Taz pathways (11, 12, 14, 15, 48), but the molecular mechanisms whereby β1 integrin interacts with each of these pathways in the lung remains largely undefined. In other organs, β1 integrin-containing integrins have been reported to negatively regulate epithelial proliferation, with an EGFR-activation dependent mechanism identified in the intestinal epithelium (49). Our data supports that β1 integrin restricts AT2 cell number as deletion leads to excessive and persistent proliferation with LPS injury. Taken together, these findings suggest that β1 integrin regulates epithelial proliferation in a cell-type specific manner during repair and that β1 integrin restricts proliferative potential in AT2s in the injured distal lung.

Historically, cellular identity has been defined by histological shape and directly observable characteristics of function (e.g., lamellar body synthesis by electron microscopy). With the advent of single-cell transcriptomics, we have increased the granularity with which we

can group similar cells together. While this technological advance has augmented our understanding of cellular transitional states, the question of how to define groups of similar cells and even the definition of cellular identity has become less clear. Indeed, repair after injury in the adult lung likely recapitulates development to regenerate new alveoli, illustrated by the similarity between the transitional cells present in normal development and the post-injury intermediate cells. Transcriptomic data demonstrated divergent AT2 to AT1 cell transition in $\beta1^{rtTA}$ lungs, consistent with the histological finding of overabundant, larger, and rounder AT2s with the loss of β1 integrin, suggesting cells that appear stuck in a transitional state in late repair. Previously published injury models report similar transitional cell states after bleomycin injury and other inflammatory stimuli (9, 10), which are marked by high *Krt8* expression, like the transitional cells in this study. The transcriptomic data in our study has some similarities and differences with recently published single-cell sequencing data from LPS injury (8). The precise mechanism by which β1 integrin governs the cellular switch in AT2 cells toward differentiation remains unknown, and future work to understand this finding could potentially identify therapeutic targets to promote differentiation after severe respiratory illness.

In conclusion, this study shows that loss of β1 integrin results in abnormal alveolar repair following LPS-induced lung injury. Repopulation of the alveolar barrier following injury requires β1 integrin-dependent regulation of AT2 proliferation and changes in epithelial cell shape. We propose that regulation of RhoA GTPase activation by β1 integrin is required for actin-rich cellular extensions, without which normal AT2 to AT1 differentiation cannot occur.

Methods

Mice and LPS injury: We induced β1 integrin in AT2 cells in the adult murine lung by crossing transgenic mice with inducible Cre recombinase expression by the doxycycline-inducible reverse tetracycline transactivator under control of the SP-C promoter (SP-C rtTA; Tet-O-Cre) with integrin $\beta1^{flox/flox}$ ($\beta1^{f/f}$) mice (50, 51). Doxycycline drinking water (2 g/L) was administered for 4 weeks beginning at P28 to triple transgenic SP-C rtTA; Tet-O-Cre; $\beta1^{f/f}$ mice (called $\beta1^{rtTA}$ mice) and littermate $\beta1^{f/f}$ controls, as previously described (17). To test the role of β1 integrin in alveolar repair, we challenged 3-month-old $\beta1^{rtTA}$ and $\beta1^{f/f}$ mice with a single intratracheal dose of LPS or PBS (3 μg/g mouse weight, equivalent volume for PBS) and harvested tissue at the indicated dates. For indicated experiments, $\beta1^{rtTA}$ mice and Cre-recombinase positive controls (without floxed alleles) were crossed to mice expressing the mTmG allele. SP-C rtTA, Tet-O-Cre, and mTmG mice were purchased from Jackson Laboratory. Integrin $\beta1^{f/f}$ mice were generously gifted by Elaine Fuchs (Howard Hughes Medical Institute, The Rockefeller University, New York, NY). All mice were maintained on the C57BL/6 background.

Histology and morphological analysis: For histological analysis on paraffin sections, mice were sacrificed, right ventricle was flushed with PBS, and lungs were inflation fixed at 25 cm with 10% formalin. After paraffin processing, embedding and sectioning, lungs were hematoxylin and eosin stained for morphological analysis by mean linear intercept, which was calculated from images (≥ 10 non-overlapping images per mouse) obtained using a x40 objective on a Keyence BZ-X710 inverted fluorescence phase contrast microscope. Immunofluorescence staining was performed on paraffin or frozen sections, as indicated. Frozen blocks were prepared from lung sections inflation fixed with a 2:1 PBS/O.C.T. (Tissue-Tek) mixture, embedded, and sectioned at

either 8 μm or 50 μm thickness. Frozen section slides were then fixed with 4% paraformaldehyde, permeabilized with .1% Triton-X, and blocked with 5% donkey serum for 2 hours at 37 degrees. Slides were incubated in primary antibody overnight at 4 degrees, followed by secondary antibody incubation for 2 hours at room temperature. For sequential primary antibody staining, a second intervening blocking step was utilized. Nuclei were stained with Dapi, ProLong Gold mountant was applied, and imaged. High power images were obtained using a Nikon Spinning Disk TiE inverted fluorescent confocal microscope attached to an Andor DU-897 EMCCD camera (x100 objective, 8 μm sections). All other images were obtained using the Keyence BZ-X710 microscope as above. The following primary antibodies and probes were used: anti-pro-SP-C (Abcam ab90716), anti-T1α (podoplanin, Developmental Studies Hybridoma Bank 8.1.1), anti-ezrin (Cell Signaling Technologies 3145S), anti-cytokeratin 8 (Invitrogen PA5-24607), and anti-Ki67-FITC (eBioscience 11-5698-90), anti-CD68 (Abcam ab125212), anti-Ager (R and D AF1145), JLA20 (Developmental Studies Hybridoma Bank JLA20-s), and phalloidin (Invitrogen A12380). We applied the following secondary antibodies: anti-rabbit Alexa Fluor 594 (Life Technologies A21207), anti-hamster Alexa Fluor 488 (Life Technologies A21110), anti-rabbit Alexa Fluor 488 (Life Technologies A21206), and anti-rabbit Alexa Fluor 647 (Life Technologies A32795). TUNEL staining was performed on paraffin sections co-immunostained with pro-SP-C, per manufacturer's kit instructions (Roche 11684795910). Quantification of immunostained sections was performed on ≥ 10 nonoverlapping images obtained with a 40x objective. JLA20 and phalloidin was quantified on lung sections (10 sections/ mouse) imaged with equivalent settings using the corrected total cell fluorescence feature from ImageJ, which corrects fluorescence integrated density for the area of the region of interest (pro-SPC+ cells).

Cell morphometry: AT2 cell area and roundness was calculated using the shape descriptor feature of ImageJ with pro-SP-C used to define the region of interest.

Bronchoalveolar lavage: After sacrifice, lungs were lavaged with 1 ml sterile PBS. The cells present in lavage fluid were collected by centrifugation, resuspended, and counted. Protein content in lavage fluid was measured by BCA protein assay (Pierce cat #23225) per manufacturer's instructions.

AEC isolation and GLISA assay: Primary AT2 cells were collected at indicated time points as previously described (17, 25), which yields > 90% AT2s (52, 53). Briefly, single cell lung suspension was generated after dispase digestion and serial filtration. Cells were then applied to plates coated with CD-32 and CD-45 for negative selection. Epithelial cells were then collected from medium after a 2 hour incubation. Cell lysates were then used for G-LISA small GTPase activation assay (Cytoskeleton cat# BK135), where levels of activated RhoA, Cdc42, and Rac1 were detected colorimetrically per manufacturer's instructions.

Single cell data collection: Sample collection and single cell sequencing was performed as previously described (54). Briefly, lung lobes were harvested, minced, and incubated for 30 minutes at 37°C in dissociation media (RPMI-1640 with 0.7 mg/ml collagenase XI and 30 mg/ml type IV bovine pancreatic DNase). After incubation, tissue was disassociated into a single-cell suspension by passage through a wide bore pipet tip and filtration through a 40 µm filter. The single-cell lung suspension was then counted, aliquoted, and blocked with CD-32 Fc block (BD

cat # 553142) for 20 minutes on ice. After a 2% FBS staining buffer wash, cells were incubated with the conjugated primary antibodies anti-CD45 (BD cat # 559864) and anti-Ter119 (Biolegend cat# 116211). Samples from day 21 after LPS were also incubated with anti-CD326 antibody (BD cat # 563477) for epithelial enrichment.

scRNA-seq library preparation and next-generation sequencing: scRNA-seq libraries were generated using the Chromium Single Cell 5' library preparation kits (10X Genomics) following the manufacturer's recommendations and targeting 10,000 - 20,000 cells per sample. Sequencing was performed on an Illumina Novaseq 6000. CellRanger Count v3.1 (10X Genomics) was used to align reads onto the mm10 reference genome.

Analysis of single cell sequencing data: Ambient background RNA was cleaned from the scRNA-seq data with "SoupX"(55) as described previously (54) using the following genes to estimate the non-expressing cells, calculate the contamination fraction, and adjust the gene expression counts: *Dcn*, *Bgn*, *Aspn*, *Ecm2*, *Fos*, *Hbb-bs*, *Hbb-bt*, *Hba-a1*, *Hba-a2*, *Lyz1*, *Lyz2*, *Mgp*, *Postn*, *Scgb1a1*. For all datasets, quality filtering was then used to remove cells with > 15% or < 0.1% mitochondrial mRNA, and to remove cells with < 700 detected genes. Dimensionality reduction, clustering, and visualization was performed using Seurat v4.0.5 and SCTransform v0.3.2.9008 with glmGamPoi v 1.6.0 (56-58). SCTransform was run with each sequencing run as a batch variable, and with the percentage of mitochondrial RNA as a regression variable. Further data cleaning was done to remove gene counts for *Gm42418*, which is likely a rRNA (59). Epithelial cells (*i.e. Epcam*+ cell clusters) were sorted *in silico* for downstream analysis. Epithelial cells were annotated with manual inspection of the following

marker genes: *Epcam*, *Sftpa1*, *Sftpc*, *Hopx*, *Aqp5*, *Col4a3*, *Ager*, *Foxj1*, *Dynlrb2*, *Mki67*, *Scgb1a1*, *Scgb3a2*, *Cdkn1a*, *Cldn4*, *Ascl1*, and *Scg5*. All charts and heatmaps as part of the scRNAseq analysis were generated with ggplot2, and all parts of the analysis were run in R 4.1.1.

Data integration was performed using a previously published dataset(8). Reads were downloaded from the Gene Expression Omnibus (GSE113049) and processed using CellRanger Count v3.1 with the mm10 genome, followed by dimensionality reduction, clustering, and visualization as described above. Data were integrated with non-SoupX processed data using the 'IntegrateData' function in Seurat, following the workflow for data normalized with SCTransform. Samples from all experiments were combined, and clusters were annotated using marker genes described in the initial publication (8), and other canonical marker genes.

Cell label transfer was also utilized with a second published dataset(7). The annotated data matrix (h5ad file) was accessed as directed in the analysis code published as part of the methods(7). The raw counts from this annotated dataset were then processed using the Seurat workflow described above, while maintaining the published cell annotations. The Seurat "TransferData" function was then used to transfer the cell annotations onto the dataset generated here.

A complete collection of all package versions, and code for all steps of the analysis is available at https://github.com/SucreLab.

Data availability

All sequencing data has been deposited to the NCBI GEO database, reviewer link available upon request.

Statistics: Comparison between two groups was performed by two-tailed t-test and 4-way comparison was done by one-way ANOVA. Individual *p*-values, t-values, F values, degrees of freedom, and sample size for each group is provided in **Supplemental Table 1**. ScRNA-sequencing analysis was completed as above.

Study approval: All animal experiments were approved by the Institutional Animal Care and Use Committee at Vanderbilt University Medical Center.

Author contributions: EJP conceived the study, performed in vivo experiments, histological analysis, image analysis, morphometric measurements, interpreted the data, and wrote the manuscript. JMSS designed and interpreted the scRNA-sequencing data and assisted in manuscript preparation. FB, JG, JTB, and KTF performed histological and image analysis. PMG performed in vivo experiments, histological analysis, lung and cell morphometry, and protein assays. XD and SK performed protein assays. WH, CSJ performed in vivo experiments. NMN and YL provided computational analysis of the scRNA-sequencing data. JAK assisted in interpretation of scRNA-sequencing data. SHG assisted in manuscript preparation. RZ and TSB conceived of the study, interpreted the data, and wrote the manuscript.

Acknowledgements: This work was supported by NIH grants K08 HL127102 (EJP), R03 HL 154287 (EJP), R01 HL163195 (EJP), K08 HL143051 (JMSS), P01 HL092870 (TSB), R01 HL151016 (TSB), R01 DK069921 (RZ), R01 DK127589 (RZ), R01 DK088327 (RZ), R01 HL157373 (JTB), R01 HL150617 (SHG), R01 HL153246 (JAK), R38 HL143619 (trainee: KTF), Merit Review Grant 2 I01 BX002378 (TSB), I01 BX002196, and the Parker B. Francis Family Foundation (JMSS, JJG). FB is the recipient of an American Society of Nephrology Ben J. Lipps Research Fellowship. JJG is the recipient of the Vanderbilt Faculty Research Scholars award. The authors would like to thank Matt Tyska and Christopher V.E. Wright for content expertise and Brittany Matlock, Angela Jones, Kari Seedle, Caitlin McCormick, and David Nichols for technical assistance. Experiments were performed in part through the use of the Vanderbilt Cell Imaging Shared Resource (supported by NIH grants CA68485, DK20593, DK58404, DK59637, and EY08126). ScRNA-sequencing experiments were performed utilizing

the Vanderbilt Technologies for Advanced Genomics Core facility. Flow cytometry experiments were performed in the VUMC Flow Cytometry Shared Resource (supported by the Vanderbilt Ingram Cancer Center P30 CA68485 and the Vanderbilt Digestive Disease Research Center DK058404).

References

1. Humphrey JD, Dufresne ER, and Schwartz MA. Mechanotransduction and extracellular matrix homeostasis. *Nat Rev Mol Cell Biol.* 2014;15(12):802-12.
2. Hynes RO. Integrins: bidirectional, allosteric signaling machines. *Cell.* 2002;110(6):673-87.
3. Sun Z, Guo SS, and Fassler R. Integrin-mediated mechanotransduction. *J Cell Biol.* 2016;215(4):445-56.
4. Streuli CH. Integrins as architects of cell behavior. *Mol Biol Cell.* 2016;27(19):2885-8.
5. Pozzi A, and Zent R. Extracellular matrix receptors in branched organs. *Curr Opin Cell Biol.* 2011;23(5):547-53.
6. Negretti NM, Plosa EJ, Benjamin JT, Schuler BA, Habermann AC, Jetter CS, et al. A single-cell atlas of mouse lung development. *Development.* 2021;148(24).
7. Strunz M, Simon LM, Ansari M, Kathiriya JJ, Angelidis I, Mayr CH, et al. Alveolar regeneration through a Krt8+ transitional stem cell state that persists in human lung fibrosis. *Nat Commun.* 2020;11(1):3559.
8. Riemondy KA, Jansing NL, Jiang P, Redente EF, Gillen AE, Fu R, et al. Single cell RNA sequencing identifies TGFbeta as a key regenerative cue following LPS-induced lung injury. *JCI Insight.* 2019;5.
9. Choi J, Park JE, Tsagkogeorga G, Yanagita M, Koo BK, Han N, et al. Inflammatory Signals Induce AT2 Cell-Derived Damage-Associated Transient Progenitors that Mediate Alveolar Regeneration. *Cell Stem Cell.* 2020;27(3):366-82 e7.
10. Kobayashi Y, Tata A, Konkimalla A, Katsura H, Lee RF, Ou J, et al. Persistence of a regeneration-associated, transitional alveolar epithelial cell state in pulmonary fibrosis. *Nat Cell Biol.* 2020;22(8):934-46.
11. Basil MC, Katzen J, Engler AE, Guo M, Herriges MJ, Kathiriya JJ, et al. The Cellular and Physiological Basis for Lung Repair and Regeneration: Past, Present, and Future. *Cell Stem Cell.* 2020;26(4):482-502.
12. Juul NH, Stockman CA, and Desai TJ. Niche Cells and Signals that Regulate Lung Alveolar Stem Cells In Vivo. *Cold Spring Harb Perspect Biol.* 2020;12(12).
13. Paris AJ, Hayer KE, Oved JH, Avgousti DC, Toulmin SA, Zepp JA, et al. STAT3-BDNF-TrkB signalling promotes alveolar epithelial regeneration after lung injury. *Nat Cell Biol.* 2020;22(10):1197-210.
14. Yuan T, Klinkhammer K, Lyu H, Gao S, Yuan J, Hopkins S, et al. Temporospatial Expression of Fgfr1 and 2 During Lung Development, Homeostasis, and Regeneration. *Front Pharmacol.* 2020;11:120.
15. Zhou B, Flodby P, Luo J, Castillo DR, Liu Y, Yu FX, et al. Claudin-18-mediated YAP activity regulates lung stem and progenitor cell homeostasis and tumorigenesis. *J Clin Invest.* 2018;128(3):970-84.
16. Crosby LM, and Waters CM. Epithelial repair mechanisms in the lung. *Am J Physiol Lung Cell Mol Physiol.* 2010;298(6):L715-31.
17. Plosa EJ, Benjamin JT, Sucre JM, Gulleman PM, Gleaves LA, Han W, et al. beta1 Integrin regulates adult lung alveolar epithelial cell inflammation. *JCI Insight.* 2020;5(2).

18. Saxon JA, Cheng DS, Han W, Polosukhin VV, McLoed AG, Richmond BW, et al. p52 Overexpression Increases Epithelial Apoptosis, Enhances Lung Injury, and Reduces Survival after Lipopolysaccharide Treatment. *J Immunol.* 2016;196(4):1891-9.
19. Lake BB, Codeluppi S, Yung YC, Gao D, Chun J, Kharchenko PV, et al. A comparative strategy for single-nucleus and single-cell transcriptomes confirms accuracy in predicted cell-type expression from nuclear RNA. *Sci Rep.* 2017;7(1):6031.
20. Fischer BM, Pavlisko E, and Voynow JA. Pathogenic triad in COPD: oxidative stress, protease-antiprotease imbalance, and inflammation. *Int J Chron Obstruct Pulmon Dis.* 2011;6:413-21.
21. Kaur G, and Batra S. Regulation of DNA methylation signatures on NF-kappaB and STAT3 pathway genes and TET activity in cigarette smoke extract-challenged cells/COPD exacerbation model in vitro. *Cell Biol Toxicol.* 2020;36(5):459-80.
22. Li J, Wang Z, Chu Q, Jiang K, Li J, and Tang N. The Strength of Mechanical Forces Determines the Differentiation of Alveolar Epithelial Cells. *Dev Cell.* 2018;44(3):297-312 e5.
23. Nobes CD, and Hall A. Rho, rac, and cdc42 GTPases regulate the assembly of multimolecular focal complexes associated with actin stress fibers, lamellipodia, and filopodia. *Cell.* 1995;81(1):53-62.
24. Takashimizu Y, and Iiyoshi M. New parameter of roundness R: circularity corrected by aspect ratio. *Progress in Earth and Planetary Science.* 2016;3(1):2.
25. Plosa EJ, Young LR, Gulleman PM, Polosukhin VV, Zaynagetdinov R, Benjamin JT, et al. Epithelial beta1 integrin is required for lung branching morphogenesis and alveolarization. *Development.* 2014;141(24):4751-62.
26. Schwartz MA, and Ginsberg MH. Networks and crosstalk: integrin signalling spreads. *Nat Cell Biol.* 2002;4(4):E65-8.
27. DiPersio CM, Hodivala-Dilke KM, Jaenisch R, Kreidberg JA, and Hynes RO. alpha3beta1 Integrin is required for normal development of the epidermal basement membrane. *J Cell Biol.* 1997;137(3):729-42.
28. DiPersio CM, van der Neut R, Georges-Labouesse E, Kreidberg JA, Sonnenberg A, and Hynes RO. alpha3beta1 and alpha6beta4 integrin receptors for laminin-5 are not essential for epidermal morphogenesis and homeostasis during skin development. *J Cell Sci.* 2000;113 (Pt 17):3051-62.
29. Yazlovitskaya EM, Tseng HY, Viquez O, Tu T, Mernaugh G, McKee KK, et al. Integrin alpha3beta1 regulates kidney collecting duct development via TRAF6-dependent K63-linked polyubiquitination of Akt. *Mol Biol Cell.* 2015;26(10):1857-74.
30. Yazlovitskaya EM, Viquez OM, Tu T, De Arcangelis A, Georges-Labouesse E, Sonnenberg A, et al. The laminin binding alpha3 and alpha6 integrins cooperate to promote epithelial cell adhesion and growth. *Matrix Biol.* 2019;77:101-16.
31. Kreidberg JA, Donovan MJ, Goldstein SL, Rennke H, Shepherd K, Jones RC, et al. Alpha 3 beta 1 integrin has a crucial role in kidney and lung organogenesis. *Development.* 1996;122(11):3537-47.
32. Menko AS, Kreidberg JA, Ryan TT, Van Bockstaele E, and Kukuruzinska MA. Loss of alpha3beta1 integrin function results in an altered differentiation program in the mouse submandibular gland. *Dev Dyn.* 2001;220(4):337-49.
33. Chen J, and Krasnow MA. Integrin Beta 1 suppresses multilayering of a simple epithelium. *PLoS One.* 2012;7(12):e52886.

34. Chen H, Bai C, and Wang X. The value of the lipopolysaccharide-induced acute lung injury model in respiratory medicine. *Expert review of respiratory medicine.* 2010;4(6):773-83.
35. Brass DM, Hollingsworth JW, Cinque M, Li Z, Potts E, Toloza E, et al. Chronic LPS inhalation causes emphysema-like changes in mouse lung that are associated with apoptosis. *Am J Respir Cell Mol Biol.* 2008;39(5):584-90.
36. Ghorani V, Boskabady MH, Khazdair MR, and Kianmeher M. Experimental animal models for COPD: a methodological review. *Tob Induc Dis.* 2017;15:25.
37. Ishii T, Hosoki K, Nikura Y, Yamashita N, Nagase T, and Yamashita N. IFN Regulatory Factor 3 Potentiates Emphysematous Aggravation by Lipopolysaccharide. *J Immunol.* 2017;198(9):3637-49.
38. Shu J, Lu W, Yang K, Zheng Q, Li D, Li Y, et al. Establishment and evaluation of chronic obstructive pulmonary disease model by chronic exposure to motor vehicle exhaust combined with lipopolysaccharide instillation. *Exp Physiol.* 2018;103(11):1532-42.
39. Singla E, Puri G, Dharwal V, and Naura AS. Gallic acid ameliorates COPD-associated exacerbation in mice. *Mol Cell Biochem.* 2021;476(1):293-302.
40. Wright JL, and Churg A. Animal models of COPD: Barriers, successes, and challenges. *Pulm Pharmacol Ther.* 2008;21(5):696-8.
41. Santa-Cruz Mateos C, Valencia-Exposito A, Palacios IM, and Martin-Bermudo MD. Integrins regulate epithelial cell shape by controlling the architecture and mechanical properties of basal actomyosin networks. *PLoS Genet.* 2020;16(6):e1008717.
42. Dominguez-Gimenez P, Brown NH, and Martin-Bermudo MD. Integrin-ECM interactions regulate the changes in cell shape driving the morphogenesis of the Drosophila wing epithelium. *J Cell Sci.* 2007;120(Pt 6):1061-71.
43. Randles MJ, Lausecker F, Humphries JD, Byron A, Clark SJ, Miner JH, et al. Basement membrane ligands initiate distinct signalling networks to direct cell shape. *Matrix Biol.* 2020;90:61-78.
44. Ron A, Azeloglu EU, Calizo RC, Hu M, Bhattacharya S, Chen Y, et al. Cell shape information is transduced through tension-independent mechanisms. *Nat Commun.* 2017;8(1):2145.
45. Hunter MP, and Zegers MM. Pak1 regulates branching morphogenesis in 3D MDCK cell culture by a PIX and beta1-integrin-dependent mechanism. *Am J Physiol Cell Physiol.* 2010;299(1):C21-32.
46. Muller PM, Rademacher J, Bagshaw RD, Wortmann C, Barth C, van Unen J, et al. Systems analysis of RhoGEF and RhoGAP regulatory proteins reveals spatially organized RAC1 signalling from integrin adhesions. *Nat Cell Biol.* 2020;22(4):498-511.
47. Rawlins EL. Lung epithelial progenitor cells: lessons from development. *Proceedings of the American Thoracic Society.* 2008;5(6):675-81.
48. Liberti DC, Kremp MM, Liberti WA, 3rd, Penkala IJ, Li S, Zhou S, et al. Alveolar epithelial cell fate is maintained in a spatially restricted manner to promote lung regeneration after acute injury. *Cell Rep.* 2021;35(6):109092.
49. Xu C, Li X, Topham MK, and Kuwada SK. Regulation of sonic hedgehog expression by integrin beta1 and epidermal growth factor receptor in intestinal epithelium. *IUBMB Life.* 2014;66(10):694-703.

50. Perl AK, Tichelaar JW, and Whitsett JA. Conditional gene expression in the respiratory epithelium of the mouse. *Transgenic Res.* 2002;11(1):21-9.
51. Raghavan S, Bauer C, Mundschau G, Li Q, and Fuchs E. Conditional ablation of beta1 integrin in skin. Severe defects in epidermal proliferation, basement membrane formation, and hair follicle invagination. *J Cell Biol.* 2000;150(5):1149-60.
52. Rice WR, Conkright JJ, Na CL, Ikegami M, Shannon JM, and Weaver TE. Maintenance of the mouse type II cell phenotype in vitro. *Am J Physiol Lung Cell Mol Physiol.* 2002;283(2):L256-64.
53. Young LR, Gulleman PM, Bridges JP, Weaver TE, Deutsch GH, Blackwell TS, et al. The alveolar epithelium determines susceptibility to lung fibrosis in Hermansky-Pudlak syndrome. *Am J Respir Crit Care Med.* 2012;186(10):1014-24.
54. Schuler BA, Habermann AC, Plosa EJ, Taylor CJ, Jetter C, Negretti NM, et al. Age-determined expression of priming protease TMPRSS2 and localization of SARS-CoV-2 in lung epithelium. *J Clin Invest.* 2021;131(1).
55. Young MD, Behjati S. . SoupX removes ambient RNA contamination from droplet based single-cell RNA sequencing data. *bioRxiv.* 2020;303727.
56. Hao Y, Hao S, Andersen-Nissen E, Mauck WM, 3rd, Zheng S, Butler A, et al. Integrated analysis of multimodal single-cell data. *Cell.* 2021;184(13):3573-87 e29.
57. Hafemeister C, and Satija R. Normalization and variance stabilization of single-cell RNA-seq data using regularized negative binomial regression. *Genome Biol.* 2019;20(1):296.
58. Ahlmann-Eltze C, and Huber W. glmGamPoi: fitting Gamma-Poisson generalized linear models on single cell count data. *Bioinformatics.* 2021;36(24):5701-2.
59. Kimmel JC, Hwang AB, Scaramozza A, Marshall WF, and Brack AS. Aging induces aberrant state transition kinetics in murine muscle stem cells. *Development.* 2020;147(9).